

Received: 27.12.2024

Accepted: 04.03.2025

Research Article

Rosemary Essential Oil as a Sustainable Corrosion Inhibitor for Copper: Quantum Chemical Insights, Characterization, Adsorption Mechanisms applying Monte Carlo, and POM analysis

**WAFAA ZRIOUEL^{a,1}, HASSAN MABRAK^b, MOHAMMED OUBAHOU^b, AZIZ BENTIS^c,
BELKHEIR HAMMOUTI^d**

^aLaboratory of Engineering and Materials (LIMAT), Faculty of Sciences Ben M'sick, Hassan II University of Casablanca, 7955, Casablanca, Morocco

^bLaboratory of Physical Chemistry of Materials, Faculty of Sciences Ben M'sick, Hassan II University of Casablanca, 7955, Casablanca, Morocco

^cMulti-laboratory LC2A, N °182 Industrial zone, Mohammedia, Morocco

^dEuro-Mediterranean University of Fes, BP 51, Fes 30070, Morocco

Abstract: This study investigates the corrosion inhibition potential of rosemary essential oil (REO) as a green, sustainable alternative for corrosion protection. The study's importance aims to evaluate new environmentally friendly corrosion inhibitors to replace traditional toxic compounds. Computational techniques, including Density Functional Theory (DFT), Mulliken atomic charge analysis, and Monte Carlo simulations, were employed to explore the adsorption mechanisms of REO components on metal surfaces. The chemical composition analysis revealed eucalyptol (49.01%), alpha-pinene (17.31%), and beta-caryophyllene (6.42%) as the major constituents. Key results showed that compounds such as alpha-thujene, beta-myrcene, and alpha-pinene are strong corrosion inhibitors, attributed to their electron-donating properties and favorable electronic characteristics. Mulliken charge analysis emphasized the critical role of oxygenated compounds, particularly alpha-terpineol, which interacts strongly with metal surfaces. Monte Carlo simulations identified gamma-cadinene as the most promising inhibitor, exhibiting the highest adsorption energies in both gas (-53.259 kJ/mol) and aqueous (-631.011 kJ/mol) phases, indicating robust interactions with copper. Additional OSIRIS and Molinspiration analyses confirmed the environmental safety and balanced lipophilicity of these molecules, further supporting their corrosion inhibition potential. The results demonstrate that REO's inhibition effect arises from both physical and chemical adsorption mechanisms, with potential synergistic effects between its constituents. This study goes beyond previous efforts by providing comprehensive computational insights into the behavior of REO, offering a foundation for future experimental validation and the development of REO as a sustainable corrosion inhibitor.

Keywords: DFT, Monte Carlo simulation, Corrosion inhibitor, Rosemary essential oil, Chromatography characterization, POM analysis

1. Introduction

Copper and its alloys are extensively utilized in diverse industrial applications, such as electrical wiring, plumbing, heat exchangers, and marine environments, due to their excellent electrical and thermal conductivity, and resistance to atmospheric corrosion [1-5]. However, despite these advantageous properties, copper remains

susceptible to corrosion in aggressive environments, such as acidic, alkaline, or chloride-rich media. This corrosion can lead to material degradation, reduced performance, and significant economic losses in the long term [6-8]. Corrosion of copper typically occurs through an electrochemical process, where the metal undergoes oxidation and dissolution in the presence

¹ Corresponding Authors

e-mail: wafaa.zriouel@gmail.com

WAFAA ZRIOUEL, HASSAN MABRAK, MOHAMMED OUBAHOU, AZIZ BENTIS,
BELKHEIR HAMMOUTI

of electrolytes. In environments containing chloride ions, for example, the corrosion rate can be significantly accelerated due to the formation of soluble copper-chloride complexes, which promote further dissolution and pitting on the metal surface [9]. To mitigate the harmful effects of copper corrosion, several studies have been carried out, in recent years, to develop new green inhibitors made from organic materials like plant extract. The use of this type of inhibitor is a promising alternative to remedy the environmental problems encountered when employing conventional corrosion inhibitors (environmental impact, health risks, limited biodegradability, high cost...etc) [10-13]. Essential oils contain a rich mixture of various organic compounds from different chemical families, including aldehydes, ketones, carboxylic acids, esters, and hydrocarbons. The presence of heteroatoms (N, O, S), aromatic rings, unsaturated double bonds, or aliphatic conjugated bonds in these compounds enhances their ability to act as effective corrosion inhibitors [11, 14-16]. To date, several plant extracts have been studied as green corrosion inhibitors namely *Camellia chrysantha* flower [17] and *Fructus cannabidis* [18] for Q235 steel corrosion, *Rosa langevita* extract for copper corrosion [19], *Cumin* essential oil [20] and *Blue Tansy* essential oil for mild steel corrosion [21], *Chamaerops humilis* L. fruit extract [22] and Hexane extract of *Nigella sativa* L for steel corrosion [23] as well as other studies. In the present work, the aim is to predict and study the inhibitory behavior, at the intermolecular scale, of the REO from Morocco. This essential oil has been the subject of several research studies evaluating its anticancer, antimicrobial and antioxidant activities [24-26], as well as its biological and pharmaceutical properties [27]. Moreover, REO has been investigated for its ability to inhibit the corrosion of copper [28] and carbon steel corrosion [29-30]. The essential oil of rosemary (REO) which is the subject of our study is rich in eucalyptol, also known as 1,8-cineole, which is a monoterpene with well-documented anti-inflammatory properties [31]. Research has shown that 1,8-cineole has exhibited a dose-dependent inhibition of monocyte mediator production at therapeutic plasma concentrations in vitro, highlighting its significance in controlling inflammation [31-33]. Additionally, 1,8-cineole has demonstrated activity against multidrug-

resistant (MDR) bacteria [33], indicating its versatile bioactivity. These properties suggest that eucalyptol could play a principal role in the corrosion inhibition of copper by REO, potentially enhancing the oil's protective effects on metal surfaces.

Despite the invaluable role of experimental studies in elucidating corrosion inhibition mechanisms and assessing the inhibition efficacy of molecules, they are often costly and time-consuming. In contrast, theoretical studies offer a powerful and efficient alternative by predicting molecular reactivity and interaction descriptors. Using molecular modeling software [34-35], chemists and engineers can predict key molecular parameters such as the energy of the highest occupied molecular orbital (EHOMO), the energy of the lowest unoccupied molecular orbital (ELUMO), the energy gap (ΔE), electronegativity (χ), chemical potential (μ), chemical hardness (η), electrophilicity index (ω), nucleophilicity (ϵ), proton affinity (PA), and softness.

In the present work, we have applied density functional theory (DFT) to calculate the quantum parameters of REO molecules to understand their reactivity. Mulliken atomic charges were determined to analyze charge distribution and molecular reactivity. Monte Carlo simulations were also carried out to model the adsorption behavior of these molecules on the copper surface. Finally, we performed a Petra/Osiris/Molinspiration analysis to evaluate potential toxicity risks and the bioactivity scores of the molecules.

2. Computational Method

2.1. Characterization of REO

The chemical composition of REO was analyzed using gas chromatography on a Clarus 580 PerkinElmer GC system equipped with a flame ionization detector (FID). A RESTEK column (60 m, 0.25 mm ID, 0.25 μ m) was utilized for the chromatographic separation. The detailed analytical conditions are summarized in Table 1.

2.2. Quantum parameters calculations

To investigate the electronic properties of the molecules, present in REO, computational methods were employed using Density Functional Theory (DFT) using the functional Hybrid/B3LYP in the Dmol3 module of the Materials Studio software

WAFAA ZRIOUEL, HASSAN MABRAK, MOHAMMED OUBAHOU, AZIZ BENTIS,
BELKHEIR HAMMOUTI

(version 2020) [36-37]. Full geometry optimizations were performed for each compound, followed by the calculation of their quantum parameters to assess the tendency of molecules to donate or accept electrons, which is crucial for understanding their interaction with the metal surface. The calculated quantum chemical parameters include the energies of the Highest Occupied Molecular Orbital (HOMO) and Lowest

Unoccupied Molecular Orbital (LUMO), electron affinity (EA), ionization potential (IP), the electronic energy gap ($\Delta\epsilon$), along with absolute electronegativity (χ), hardness (η), softness (σ) and the electrophilicity index. These parameters were determined using relationships derived from Koopmans' theorem, as previously reported in the literature [38-41].

Table 1. Analytical conditions of the characterization of REO using GC/FID

Injection volume	1 μ l		
Injector temperature	250 C (split with split ratio of 5)		
Detector temperature (FID)	280 C		
Column	RESTEK (60 m, 0.25 mm ID, 0.25 μ m)		
Detector	FID		
Carrier gas	N, H et Air 1.2, 45 et 450ml/min respectively		
Oven program	°C/min	Temperature (°C)	Maintain (min)
	...	50	5
	10	200	0
	5	240	2

$$IP = -\epsilon_{HOMO} \quad (1)$$

$$EA = -\epsilon_{LUMO} \quad (2)$$

$$\Delta\epsilon = \epsilon_{LUMO} - \epsilon_{HOMO} \quad (3)$$

$$\chi = -\mu_i = -\left(\frac{\epsilon_{LUMO} + \epsilon_{HOMO}}{2}\right) \quad (4)$$

$$\eta = \frac{\epsilon_{LUMO} - \epsilon_{HOMO}}{2} \quad (5)$$

$$\sigma = \frac{1}{\eta} = \frac{2}{\epsilon_{LUMO} - \epsilon_{HOMO}} \quad (6)$$

$$\omega = \frac{\chi^2}{2\eta} \quad (7)$$

2.3. Mulliken atomic charges

Mulliken population analysis is a widely used technique for identifying potential adsorption sites of inhibitors, providing valuable insights into the electronic structure and reactivity of molecules [42]. This method allows for the calculation of atomic charges, bond orders, and electron density distribution, to understand how molecules interact with surfaces. These charges are derived from the molecular wavefunction by summing up the electron populations in atomic orbitals and accounting for charge transfer between atoms. A positive Mulliken charge indicates electron deficiency, making the atom more likely to accept electrons (acting as an electrophilic site), whereas a negative charge suggests electron richness,

increasing its tendency to donate electrons (nucleophilic site). This charge distribution is particularly important in corrosion inhibition studies, where adsorption onto a metal surface is influenced by electrostatic interactions between the inhibitor's charged sites and the metal atoms. Functional groups containing electronegative elements (such as oxygen, nitrogen, and sulfur) often acquire negative Mulliken charges, enhancing their ability to form strong interactions with positively charged metal centers. Conversely, less electronegative atoms may exhibit positive charges, affecting the molecule's overall adsorption orientation and bonding strength [43-45]. The Mulliken atomic charges of the all of molecules comprising in the REO are calculated using the

WAFAA ZRIOUEL, HASSAN MABRAK, MOHAMMED OUBAHOU, AZIZ BENTIS,
BELKHEIR HAMMOUTI

Dmol³ module of Material Studio software version 2020 [36].

2.4. Monte Carlo simulation

Monte Carlo simulation is a powerful computational technique used in the study of corrosion inhibition to predict and analyze the interaction between inhibitor molecules and metal surfaces. By employing statistical sampling methods, this approach simulates the adsorption behavior of inhibitors on metal surfaces, considering various molecular orientations and conformations [46]. In corrosion inhibition studies, Monte Carlo simulations provide insights into the adsorption mechanisms at the atomic level, aiding in the evaluation of inhibitor efficiency and the design of more effective corrosion inhibitors. For each molecule of REO, we perform a geometric optimization using the Forcite module of Material Studio software version 2020. After this optimization, we use the adsorption Locator module to simulate the all of configurations of the adsorption and the interaction between all of the molecules and the copper surface, specifically the Cu (1 1 1) surface, which was chosen for the simulation due to its stability, in the gas and aqueous phases [47-49].

2.5. The Petra/Osiris/Molinspiration

The POM (Petra/Osiris/Molinspiration) theory, developed by the research group of Taibi Ben Hadda in collaboration with the American National

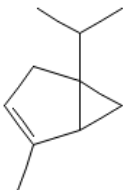
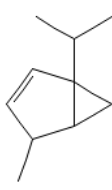
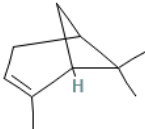
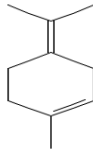
Cancer Institute (NCI) and the Therapeutic and Antiviral Screening Center (TAACF), has significantly advanced the fields of pharmacology and drug design [50]. This theory combines the computational tools Petra, Osiris, and Molinspiration to comprehensively evaluate molecular properties. It aims to identify pharmacophore sites within the studied molecules, explain or predict their biological activity, and propose structural modifications to improve the molecule's performance [51-52]. The POM analysis is a valuable approach for studying new green corrosion inhibitors, using Petra, Osiris, and Molinspiration to evaluate key molecular properties. Petra focuses on electronic parameters like molecular orbital energies and charge distribution, essential for understanding reactivity and adsorption. Osiris assesses properties such as lipophilicity, toxicity, and solubility to evaluate environmental safety, while Molinspiration calculates descriptors like topological polar surface area and logP values to determine the hydrophobic or hydrophilic nature [53-54].

3. Results and discussion

3.1. Characterization of REO

The results of the characterization of the studied REO, using the GC/FID, are presented in the Table 2.

Table 2. Chemical composition of REO obtained by GC-FID

Molecule	Structure of compound	Percentage %	Molecule	Structure of compound	Percentage %
Alpha-Thujene C ₁₀ H ₁₆		0.53	Beta-thujene C ₁₀ H ₁₆		0.26
Alpha-pinene C ₁₀ H ₁₆		17.31	Terpinolene C ₁₀ H ₁₆		0.87

WAFAA ZRIOUEL, HASSAN MABRAK, MOHAMMED OUBAHOU, AZIZ BENTIS,
BELKHEIR HAMMOUTI

Table 2. Chemical composition of REO obtained by GC-FID

Molecule	Structure of compound	Percentage %	Molecule	Structure of compound	Percentage %
Camphene $C_{10}H_{16}$		3.75	Eucalyptol $C_{10}H_{18}O$		49.01
Beta-myrcene $C_{10}H_{16}$		1.81	Gamma-terpinene $C_{10}H_{16}$		1.39
O-cymene $C_{10}H_{14}$		0.77	Alpha-terpinolene $C_{10}H_{16}$		0.51
Linalool $C_{10}H_{18}O$		1.01	Isoborneol $C_{10}H_{18}O$		3.82
Terpinen-4-ol $C_{10}H_{18}O$		0.8	Terpineol $C_{10}H_{18}O$		3.25
Borneol acetate $C_{12}H_{20}O_2$		1.15	Beta-caryophyllène $C_{15}H_{24}O$		6.42
Humulene $C_{15}H_{24}$		0.76	Gamma-cadinene $C_{15}H_{24}$		0.81
Alpha-terpineol $C_{10}H_{18}O$		2.47			

The chemical composition of REO was determined to assess its potential as a green corrosion inhibitor. The analysis revealed that eucalyptol (49.01%) is the dominant component, followed by alpha-pinene (17.31%) and beta-caryophyllene (6.42%). The dominant molecule in REO, the eucalyptol or 1.8-cineol, is known for its antimicrobial and

antioxidant properties [55-58], suggesting that it may be a potential corrosion inhibitor by blocking or slowing the oxidation reactions. The mechanism by which eucalyptol might inhibit corrosion could involve its ability to adsorb onto the metal surface and form a protective film [59]. This film acts as a physical barrier, preventing aggressive corrosive

**WAFAA ZRIOUEL, HASSAN MABRAK, MOHAMMED OUBAHOU, AZIZ BENTIS,
BELKHEIR HAMMOUTI**

agents, such as chloride ions in acidic solutions, from reaching the metal surface. The high concentration of eucalyptol suggests it may be the key molecule for corrosion inhibition by REO. The second dominant component, in the chemical composition of the REO studied, is alpha-pinene which is a hydrophobic terpene [60-61]. Although alpha-pinene presents certain risks to human health and to the environment, it has been applied in controlling waste gas emissions, offering several economic and environmental advantages over conventional physicochemical technologies like absorption, adsorption, catalytic oxidation, scrubbing, and thermal treatment [62]. Its high concentration (17.31%) in REO indicates that its potential benefits in corrosion inhibition should not be neglected. The hydrophobic nature of alpha-pinene minimizes water contact with the metal surface, thereby reducing electrochemical reactions responsible for corrosion [63-64]. The third principal molecule of the REO is the bicyclic sesquiterpene: beta-Caryophyllene, which offers numerous medicinal benefits like anti-inflammatory, Antidepressant, and antioxidant properties [65-67]. Due to its bulkiness, it can enhance the formation of a dense protective film on the metal, effectively blocking the diffusion of corrosive species like hydrogen ions or chloride ions. In addition to these main molecules, we find other molecules with other functional groups such as alcohols (Isoborneol (3.82%) and Terpineol (3.25%)), these alcohols possess hydroxyl groups (-OH) that can interact with the metal surface via hydrogen bonding or chemisorption, which strengthens the oil's adsorption onto the surface. The presence of polar functional groups in these molecules enhances their affinity for the metal surface, which could improve the protective film's stability and reduce corrosion. For the minor components like camphene, linalool and terpene, their synergy can be attributed to the slowing down of corrosion.

3.2. Quantum parameters calculation

The DFT calculations are based on a fixed molecular structure and do not account for dynamic atomic motions or temperature-induced fluctuations, which could influence the behavior of molecules in real conditions. The quantum parameters of the molecules of the REO, including

the highest occupied molecular orbital (HOMO) energy, lowest unoccupied molecular orbital (LUMO) energy, energy gap (ΔE), electronegativity (χ), hardness (η), and electrophilicity index (ω), are summarized in Table 3. These parameters provide insight into the electronic properties and reactivity of the molecules. Additionally, Table 4 presents the optimized molecular geometries, illustrating the most stable conformations, along with visual representations of the HOMO and LUMO orbitals. From the quantum chemical parameters in Table 3, alpha-thujene (-5.06 eV) and alpha-pinene (-5.201 eV) exhibit the highest eHOMO values, indicating that they are the most effective electron donors. Which means that these molecules are capable of building bonds with the surface of the metal and subsequently creating a protective layer [68]. While molecules like isoborneol (-6.951 eV) and Camphene (-6.812 eV) have significantly lower eHOMO values, suggesting they are weaker electron donors and may be less effective as inhibitors through electron donation.

Based the results of the lowest unoccupied molecular orbital (eLUMO), Isoborneol (2.237 eV) and Eucalyptol (1.768 eV) have the highest eLUMO values among the components, indicating a strong potential to accept electrons from the metal surface, which can enhance inhibition efficiency. On the other hand, molecules like Terpinene-4-ol (0.29 eV) and beta-myrcene (0.267 eV) have much lower eLUMO values, indicating lower electron-accepting capacities, which might affect their overall reactivity in corrosion inhibition [69-70].

Regarding chemical reactivity, beta-myrcene shows the smallest energy gap (5.597 eV), suggesting that it is the most chemically reactive molecule, which enhances its ability to inhibit corrosion by facilitating electron exchange [71]. On the contrary, isoborneol (9.188 eV) and Eucalyptol (8.489 eV) have the largest energy gaps, indicating that these molecules are more stable and less reactive [72-73].

Alpha-thujene (1.693 eV) and alpha-pinene (1.761 eV) have the lowest electronegativity values, making them strong electron donors. This property is beneficial for adsorption onto the metal surface, facilitating the formation of a protective film. In contrast, molecules like Camphene (3.172 eV) and isoborneol (2.357 eV) are more electronegative,

WAFAA ZRIOUEL, HASSAN MABRAK, MOHAMMED OUBAHOU, AZIZ BENTIS,
BELKHEIR HAMMOUTI

which could influence their effectiveness as inhibitors [74]. Molecular hardness (η) and softness (σ) provide insights into a molecule's resistance to deformation and reactivity. Gamma-terpinene ($\eta = 3.399$ eV, $\sigma = 0.294$ eV⁻¹) and alpha-thujene ($\eta = 3.368$ eV, $\sigma = 0.297$ eV⁻¹) have lower hardness and higher softness values, indicating that they are highly reactive and can easily interact with the metal surface [75]. To summarize the analysis of the quantum parameters, we find that alpha-thujene,

beta-myrcene and alpha-pinene are the molecules that promote corrosion inhibition based on their electron donor results, of their moderate energy differences and their higher softness. Although eucalyptol is the most dominant component, its large energy gap and hardness reduce its effectiveness as a corrosion inhibitor. Similarly, isoborneol may also have limited effectiveness due to its high hardness and low reactivity.

Table 3. Quantum parameters of all of the molecules comprising in the REO obtained by Dmol³/DFT

Parameter	%	ϵ_{HOMO}	ϵ_{LUMO}	gap	χ (eV)	η	σ	ω
		(eV)	(eV)					
Alpha-pinene	17.31	-5.201	1.679	6.88	1.761	3.440	0.291	0.451
Alpha-terpinolene	0.51	-6.133	0.609	6.742	2.762	3.371	0.297	1.132
Alpha-thujene	0.53	-5.06	1.675	6.735	1.693	3.368	0.297	0.425
Beta-myrcene	1.81	-5.33	0.267	5.597	2.532	2.799	0.357	1.145
Beta-caryophyllene	6.42	-5.391	1.382	6.773	2.005	3.387	0.295	0.593
Beta-thujene	0.26	-6.503	0.304	6.807	3.100	3.404	0.294	1.411
Borneol acetate	1.15	-6.54	0.659	7.199	2.941	3.600	0.278	1.201
Camphene	3.75	-6.812	0.469	7.281	3.172	3.641	0.275	1.381
Cineol	49.01	-6.721	1.768	8.489	2.477	4.245	0.236	0.722
Gamma-cadinene	0.81	-5.553	1.442	6.995	2.056	3.498	0.286	0.604
Gamma-terpinene	1.39	-5.2	1.598	6.798	1.801	3.399	0.294	0.477
Humulene	0.76	-6.098	0.518	6.616	2.790	3.308	0.302	1.177
Isoborneol	3.82	-6.951	2.237	9.188	2.357	4.594	0.218	0.605
Linalool	1.01	-6.1	0.36	6.46	2.870	3.230	0.310	1.275
O-cymene	0.77	-6.101	0.489	6.59	2.806	3.295	0.303	1.195
Terpinene-4-ol	0.8	-6.905	0.29	7.195	3.308	3.598	0.278	1.520
Terpineol	3.25	-5.82	1.449	7.269	2.186	3.635	0.275	0.657
Terpinolene	0.87	-6.133	0.609	6.742	2.762	3.371	0.297	1.132
Alpha-teripneol	2.47	-5.394	1.629	7.023	1.883	3.512	0.285	0.505

The table 4 highlights the HOMO and LUMO distributions of molecules constituting REO (REO), providing insights into their potential corrosion inhibition mechanisms. Molecules such as terpinen-4-ol and eucalyptol exhibit significant electron density around polar functional groups like hydroxyl and oxygen atoms, suggesting strong adsorption potential on metal surfaces. Conversely, molecules like alpha-pinene and gamma-cadinene show HOMO and LUMO densities primarily localized on nonpolar regions, indicating weaker metal interactions. Compounds with conjugated systems, such as beta-caryophyllene and gamma-

terpinene, display electron density around double bonds, which could contribute to moderate adsorption but may lack strong coordination sites. Overall, molecules with smaller energy gaps and reactive functional groups, such as terpinen-4-ol, are likely the most effective inhibitors due to their ability to form stable interactions with metal surfaces, reducing corrosion rates.

3.3. Mulliken atomic charges calculation

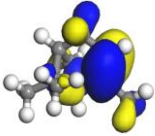
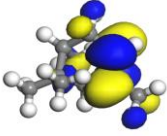
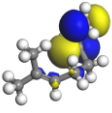
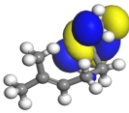
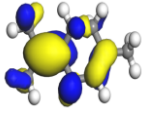
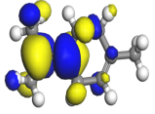
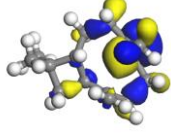
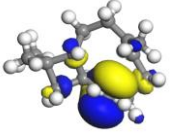
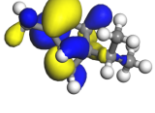
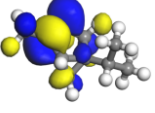
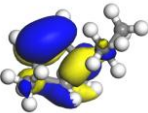
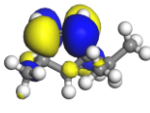
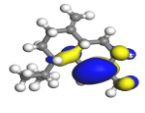
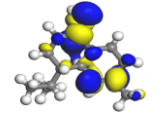
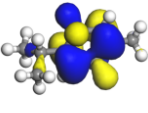
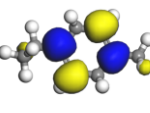
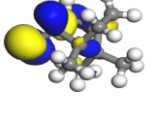
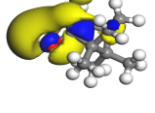
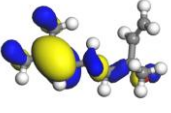
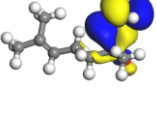
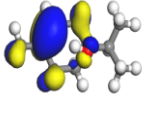
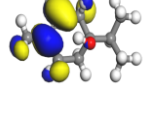
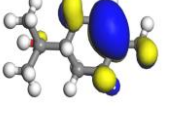
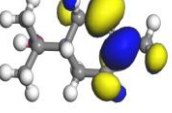
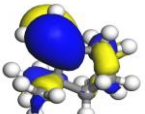
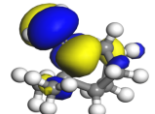
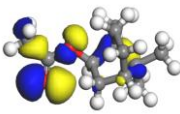
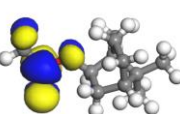

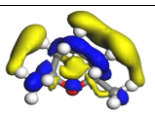
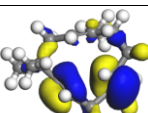
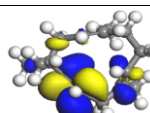
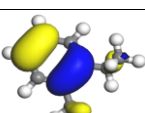
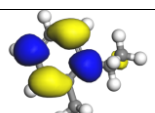
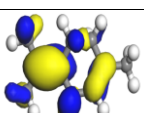
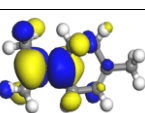
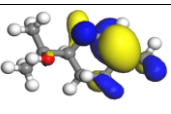
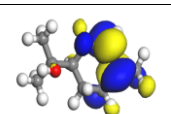
The Mulliken atomic charges of the molecules contained in REO were determined. These charges offer important insights into the electron density

WAFAA ZRIOUEL, HASSAN MABRAK, MOHAMMED OUBAHOU, AZIZ BENTIS,
BELKHEIR HAMMOUTI

distribution across individual atoms, highlighting areas of potential electrophilic or nucleophilic activity. The results, presented in Table 5, provide

a deeper understanding of the electronic characteristics of the REO molecules.

Table 4. Optimization of the geometric structures of HOMO and LUMO orbitals of all of the molecules that constitute REO

Molecule	HOMO	LUMO	Molecule	HOMO	LUMO
Alpha-pinene			Beta-Myrcene		
Alpha-terpinolene			Beta-caryophyllene		
Alpha-thujene			Beta-thujene		
Gamma-cadinene			Gamma-terpinene		
Isoborneol			Linalool		
Terpinene-4-ol			Terpineol		
Camphene			Borneol acetate		
Eucalyptol			Humulene		
O-cymene			Terpinolene		
Alpha-terpineol					

From Mulliken atomic charges calculation, we can conclude that Oxygen-containing molecules such

as borneol acetate, eucalyptol, isoborneol, linalool, terpinene-4-ol, terpineol, and alpha-terpineol

WAFAA ZRIOUEL, HASSAN MABRAK, MOHAMMED OUBAHOU, AZIZ BENTIS,
BELKHEIR HAMMOUTI

exhibit highly negative charges on their oxygen atoms. These negative charges, ranging from -0.517 to -0.697, indicate high electron density, which makes these oxygen atoms nucleophilic and capable of interacting strongly with the positively charged sites on the metal surface [76-77]. The negative oxygen charges create an electrostatic

attraction with the positively charged metal ions. Among these, alpha-terpineol stands out with the most negative oxygen charge (-0.697), suggesting that it may have the highest reactivity and the strongest adsorption potential, making it a key molecule in the inhibition process [78-79].

Table 5. Mulliken atomic charges of all of the molecules that constitute REO (1/3)

Alpha-terpineol									
Atom	Charge	Atom	Charge	Atom	Charge	Atom	Charge	Atom	Charge
O (1)	-0.697	C (7)	0.164	H (13)	0.151	H (19)	0.124	H (25)	0.142
C (2)	-0.152	C (8)	-0.188	H (14)	0.177	H (20)	0.153	H (26)	0.404
C (3)	0.292	C (9)	-0.481	H (15)	0.177	H (21)	0.141	H (27)	0.156
C (4)	-0.303	C (10)	-0.482	H (16)	0.155	H (22)	0.178	H (28)	0.153
C (5)	-0.326	C (11)	-0.506	H (17)	0.147	H (23)	0.173	H (29)	0.154
C (6)	-0.344	H (12)	0.136	H (18)	0.148	H (24)	0.153		

The non-oxygenated hydrocarbons, such as beta-caryophyllene, gamma-cadinene, and humulene, present a different picture. The atomic charges on carbon atoms in these molecules are moderately negative or positive, generally ranging from -0.033 to -0.316. These values indicate a lower potential for strong adsorption compared to the oxygen atoms in oxygen-containing compounds. However, the polarizable nature of some carbon atoms can still contribute to weak adsorption through Van der Waals interactions [80-81]. The presence of these molecules can still contribute to the stabilization of the protective film through physical adsorption.

In summary, while individual components such as alpha-terpineol and eucalyptol exhibit strong inhibitory properties due to their reactive oxygen atoms, the overall inhibition efficiency of the REO may be further enhanced by the synergistic interactions among various molecules [82-83]. The combination of chemical and physical adsorption mechanisms leads to a more comprehensive protective effect, indicating that the essential oil's corrosion inhibition is a result of both strong chemical interactions from highly reactive molecules and supportive physical adsorption from less reactive components [21].

3.4. Monte Carlo simulation

The Monte Carlo simulations were conducted to evaluate the adsorption behavior of different molecules of the REO on the copper (111) surface. The results for both gas and aqueous phases are

presented in Table 6. The total energy values represent the overall stability of the inhibitor molecules. Lower total energy values indicate more stable molecules, which are likely to interact more effectively with the metal surface, contributing to their efficiency as corrosion inhibitors. In this study, the comparison of total energy values for each molecule in the gas and aqueous phases provides insight into their relative stability. More stable molecules are expected to form stronger interactions with the metal surface, enhancing the inhibition process. The adsorption energy refers to the energy released or required when the adsorbate components, in both their relaxed and unrelaxed states, are adsorbed onto the substrate. The rigid adsorption energy indicates the energy released (or absorbed) during the adsorption of the unrelaxed adsorbate component (prior to geometry optimization) onto the substrate [84]. Finally, the deformation energy reflects the energy released when the adsorbed component of the adsorbate is relaxed on the substrate surface [85-86].

The Monte Carlo simulation results, in Table 6, show that gamma-cadinene is the most effective inhibitor in both gas and aqueous phases, with the highest adsorption energy values of -53.259 kJ/mol and -631.011 kJ/mol, respectively, indicating a strong interaction with the copper (111) surface. In the aqueous phase, humulene and alpha-terpineol also demonstrate significant adsorption energies of -631.220 kJ/mol and -630.830 kJ/mol.

Beta-caryophyllene		Gamma-cadinene		Humulene		Borneol acetate		Eucalyptol		Isoborneol		Linalool		Terpinene-4-ol		Terpineol	
Atom	Charge	Atom	Charge	Atom	Charge	Atom	Charge	Atom	Charge	Atom	Charge	Atom	Charge	Atom	Charge	Atom	Charge
C (1)	-0.033	C (1)	-0.106	C (1)	-0.069	O (1)	-0.517	O (1)	-0.518	O (1)	-0.607	O (1)	-0.584	O (1)	-0.591	O (1)	-0.591
C (2)	-0.081	C (2)	-0.065	C (2)	-0.201	O (2)	-0.468	C (2)	-0.183	C (2)	-0.048	C (2)	0.122	C (2)	0.158	C (2)	-0.088
C (3)	-0.112	C (3)	-0.148	C (3)	-0.013	C (3)	-0.047	C (3)	0.154	C (3)	-0.010	C (3)	-0.165	C (3)	-0.101	C (3)	0.151
C (4)	-0.167	C (4)	-0.184	C (4)	-0.259	C (4)	-0.009	C (4)	0.201	C (4)	-0.143	C (4)	-0.219	C (4)	-0.180	C (4)	-0.193
C (5)	-0.171	C (5)	-0.124	C (5)	-0.291	C (5)	-0.145	C (5)	-0.158	C (5)	0.150	C (5)	-0.269	C (5)	-0.224	C (5)	-0.202
C (6)	-0.273	C (6)	-0.189	C (6)	-0.100	C (6)	0.138	C (6)	-0.158	C (6)	-0.179	C (6)	-0.013	C (6)	-0.241	C (6)	-0.223
C (7)	-0.262	C (7)	0.146	C (7)	0.099	C (7)	-0.171	C (7)	-0.171	C (7)	-0.174	C (7)	-0.135	C (7)	0.092	C (7)	0.094
C (8)	0.124	C (8)	-0.221	C (8)	-0.222	C (8)	-0.143	C (8)	-0.171	C (8)	-0.149	C (8)	0.101	C (8)	-0.124	C (8)	-0.127
C (9)	-0.211	C (9)	-0.138	C (9)	-0.085	C (9)	-0.151	C (9)	-0.254	C (9)	-0.280	C (9)	-0.306	C (9)	-0.281	C (9)	- 0.283
C (10)	-0.216	C (10)	-0.230	C (10)	-0.209	C (10)	-0.295	C (10)	-0.260	C (10)	-0.270	C (10)	-0.333	C (10)	-0.271	C (10)	-0.277
C (11)	0.102	C (11)	0.087	C (11)	-0.253	C (11)	-0.284	C (11)	-0.260	C (11)	-0.282	C (11)	-0.219	C (11)	-0.314	C (11)	-0.317
C (12)	-0.180	C (12)	-0.275	C (12)	0.098	C (12)	-0.287	H (12)	0.088	H (12)	0.077	H (12)	0.087	H (12)	0.088	H (12)	0.087
C (13)	-0.271	C (13)	-0.282	C (13)	-0.088	C (13)	0.536	H (13)	0.102	H (13)	0.091	H (13)	0.110	H (13)	0.121	H (13)	0.134
C (14)	-0.151	C (14)	-0.285	C (14)	-0.350	C (14)	-0.318	H (14)	0.095	H (14)	0.107	H (14)	0.106	H (14)	0.100	H (14)	0.091
C (15)	-0.316	C (15)	-0.305	C (15)	-0.328	H (15)	0.079	H (15)	0.095	H (15)	0.090	H (15)	0.106	H (15)	0.124	H (15)	0.101
H (16)	0.089	H (16)	0.112	H (16)	0.102	H (16)	0.130	H (16)	0.102	H (16)	0.090	H (16)	0.111	H (16)	0.130	H (16)	0.140
H (17)	0.100	H (17)	0.087	H (17)	0.096	H (17)	0.129	H (17)	0.093	H (17)	0.112	H (17)	0.116	H (17)	0.127	H (17)	0.094
H (18)	0.088	H (18)	0.101	H (18)	0.069	H (18)	0.097	H (18)	0.108	H (18)	0.087	H (18)	0.101	H (18)	0.111	H (18)	0.100
H (19)	0.097	H (19)	0.100	H (19)	0.091	H (19)	0.119	H (19)	0.108	H (19)	0.099	H (19)	0.075	H (19)	0.090	H (19)	0.068
H (20)	0.090	H (20)	0.100	H (20)	0.092	H (20)	0.108	H (20)	0.093	H (20)	0.088	H (20)	0.073	H (20)	0.114	H (20)	0.098
H (21)	0.096	H (21)	0.102	H (21)	0.100	H (21)	0.098	H (21)	0.088	H (21)	0.089	H (21)	0.332	H (21)	0.095	H (21)	0.085
H (22)	0.090	H (22)	0.094	H (22)	0.097	H (22)	0.092	H (22)	0.106	H (22)	0.131	H (22)	0.100	H (22)	0.089	H (22)	0.119
H (23)	0.091	H (23)	0.101	H (23)	0.098	H (23)	0.100	H (23)	0.106	H (23)	0.082	H (23)	0.101	H (23)	0.139	H (23)	0.122
H (24)	0.087	H (24)	0.102	H (24)	0.108	H (24)	0.095	H (24)	0.086	H (24)	0.096	H (24)	0.096				

WAF AA ZRIOUEL, HASSAN MABRAK, MOHAMMED OUBAHOU, AZIZ BENTIS, BELKHEIR HAMMOUTI

Table 5. Mulliken atomic charges of all of the molecules that constitute REO (3/3)

Camphene		Terpinolene		Gamma-terpinene		Alpha-pinene		Alpha-terpinolene		Alpha-Thujene		Beta- myrcene		Beta-thujene		O-cymene	
Atom	Charge	Atom	Charge	Atom	Charge	Atom	Charge	Atom	Charge	Atom	Charge	Atom	Charge	Atom	Charge	Atom	Charge
C (1)	-0.149	C (1)	-0.245	C (1)	-0.146	C (1)	0.045	C (1)	-0.245	C (1)	-0.011	C (1)	-0.222	C (1)	-0.003	C (1)	-0.183
C (2)	-0.035	C (2)	0.052	C (2)	0.073	C (2)	-0.134	C (2)	0.052	C (2)	-0.164	C (2)	-0.243	C (2)	-0.126	C (2)	0.069
C (3)	-0.196	C (3)	-0.211	C (3)	-0.221	C (3)	-0.187	C (3)	-0.211	C (3)	-0.166	C (3)	-0.098	C (3)	-0.180	C (3)	0.040
C (4)	-0.147	C (4)	-0.226	C (4)	-0.223	C (4)	-0.132	C (4)	-0.226	C (4)	-0.181	C (4)	0.087	C (4)	-0.090	C (4)	-0.253
C (5)	-0.147	C (5)	0.083	C (5)	-0.143	C (5)	-0.153	C (5)	0.083	C (5)	-0.121	C (5)	0.134	C (5)	-0.120	C (5)	-0.253
C (6)	-0.137	C (6)	-0.129	C (6)	0.079	C (6)	0.124	C (6)	-0.129	C (6)	0.121	C (6)	-0.298	C (6)	-0.068	C (6)	-0.111
C (7)	0.164	C (7)	-0.003	C (7)	-0.137	C (7)	-0.285	C (7)	-0.003	C (7)	-0.142	C (7)	-0.333	C (7)	-0.087	C (7)	-0.108
C (8)	-0.257	C (8)	-0.303	C (8)	-0.249	C (8)	-0.288	C (8)	-0.303	C (8)	-0.259	C (8)	-0.060	C (8)	-0.256	C (8)	-0.315
C (9)	-0.257	C (9)	-0.309	C (9)	-0.249	C (9)	-0.133	C (9)	-0.309	C (9)	-0.261	C (9)	-0.246	C (9)	-0.266	C (9)	-0.094
C (10)	-0.289	C (10)	-0.307	C (10)	-0.311	C (10)	-0.304	C (10)	-0.307	C (10)	-0.322	C (10)	-0.235	C (10)	-0.270	C (10)	-0.095
H (11)	0.074	H (11)	0.094	H (11)	0.089	H (11)	0.070	H (11)	0.094	H (11)	0.087	H (11)	0.108	H (11)	0.087	H (11)	0.101
H (12)	0.078	H (12)	0.107	H (12)	0.102	H (12)	0.066	H (12)	0.107	H (12)	0.098	H (12)	0.097	H (12)	0.103	H (12)	0.095
H (13)	0.086	H (13)	0.093	H (13)	0.102	H (13)	0.083	H (13)	0.093	H (13)	0.099	H (13)	0.097	H (13)	0.099	H (13)	0.088
H (14)	0.104	H (14)	0.108	H (14)	0.100	H (14)	0.099	H (14)	0.108	H (14)	0.101	H (14)	0.101	H (14)	0.094	H (14)	0.097
H (15)	0.099	H (15)	0.113	H (15)	0.100	H (15)	0.098	H (15)	0.113	H (15)	0.109	H (15)	0.064	H (15)	0.085	H (15)	0.097
H (16)	0.090	H (16)	0.111	H (16)	0.066	H (16)	0.098	H (16)	0.111	H (16)	0.087	H (16)	0.098	H (16)	0.079	H (16)	0.088
H (17)	0.092	H (17)	0.073	H (17)	0.063	H (17)	0.093	H (17)	0.073	H (17)	0.069	H (17)	0.092	H (17)	0.076	H (17)	0.095
H (18)	0.097	H (18)	0.092	H (18)	0.091	H (18)	0.093	H (18)	0.092	H (18)	0.092	H (18)	0.098	H (18)	0.104	H (18)	0.083
H (19)	0.103	H (19)	0.102	H (19)	0.090	H (19)	0.098	H (19)	0.102	H (19)	0.086	H (19)	0.097	H (19)	0.089	H (19)	0.078
H (20)	0.086	H (20)	0.098	H (20)	0.081	H (20)	0.088	H (20)	0.098	H (20)	0.094	H (20)	0.112	H (20)	0.088	H (20)	0.112
H (21)	0.094	H (21)	0.108	H (21)	0.091	H (21)	0.088	H (21)	0.108	H (21)	0.094	H (21)	0.100	H (21)	0.094	H (21)	0.112
H (22)	0.102	H (22)	0.094	H (22)	0.091	H (22)	0.103	H (22)	0.094	H (22)	0.085	H (22)	0.083	H (22)	0.089	H (22)	0.095
H (23)	0.093	H (23)	0.106	H (23)	0.080	H (23)	0.071	H (23)	0.106	H (23)	0.094	H (23)	0.090	H (23)	0.095	H (23)	0.080
H (24)	0.087	H (24)	0.099	H (24)	0.094	H (24)	0.102	H (24)	0.099	H (24)	0.105	H (24)	0.087	H (24)	0.096	H (24)	0.080
H (25)	0.086	H (25)	0.102	H (25)	0.092	H (25)	0.103	H (25)	0.102	H (25)	0.099	H (25)	0.095	H (25)	0.086		
H (26)	0.081	H (26)	0.097	H (26)	0.095	H (26)	0.094	H (26)	0.097	H (26)	0.105	H (26)	0.094	H (26)	0.101		

WAFAA ZRIOUEL, HASSAN MABRAK, MOHAMMED OUBAHOU, AZIZ BENTIS,
BELKHEIR HAMMOUTI

Table 6. Monte Carlo simulation results of the molecules constituting REO in gas and aqueous phases

Molecule	Phases	Total energy Kcal/mol	Adsorption energy kJ/mole	Rigid adsorption energy kJ/mol	Deformation energy kJ/mol
Copper (1 1 1) + alpha pinene	Gas phase	-29.762	-29.508	-29.669	0.160
	Aqueous phase	-625.256	-625.256	-658.404	33.148
Copper (1 1 1) + alpha-thujene	Gas phase	50.505	-34.440	-35.159	0.718
	Aqueous phase	-628.975	-628.975	-661.667	32.691
Copper (1 1 1) + Beta-myrcene	Gas phase	-56.426	-46.321	-47.944	1.623
	Aqueous phase	-626.669	-626.669	-659.887	33.217
Copper (1 1 1) + Alpha-terpinolene	Gas phase	-53.656	-44.504	-47.239	2.734
	Aqueous phase	-626.598	-626.598	-660.358	33.759
Copper (1 1 1) + Beta-thujene	Gas phase	94.554	-33.524	-34.309	0.786
	Aqueous phase	-623.613	-623.613	-656.677	33.063
Copper (1 1 1) + Beta-Caryophyllene	Gas phase	-61.343	-49.086	-51.014	1.928
	Aqueous phase	-624.723	-624.723	-658.294	33.570
Copper (1 1 1) + Borneol acetate	Gas phase	-67.124	-41.158	-42.813	1.655
	Aqueous phase	-626.730	-626.730	-659.555	32.825
Copper (1 1 1) + Camphene	Gas phase	-42.541	-31.638	-31.889	0.251
	Aqueous phase	-622.464	-622.464	-655.693	33.229
Copper (1 1 1) + Eucalyptol	Gas phase	-74.269	-32.333	-32.604	0.271
	Aqueous phase	-628.844	-628.844	-660.845	32.000
Copper (1 1 1) + Gamma-cadinene	Gas phase	-88.250	-53.259	-57.243	3.985
	Aqueous phase	-631.011	-631.011	-663.849	32.837
Copper (1 1 1) + Gamma-terpinene	Gas phase	-59.170	-46.275	-46.685	0.4101
	Aqueous phase	-622.542	-622.542	-656.352	33.810
Copper (1 1 1) + Humulene	Gas phase	-61.503	-36.485	-37.144	0.658
	Aqueous phase	-631.220	-631.220	-664.666	33.446
Copper (1 1 1) + Isoborneol	Gas phase	-38.141	-27.594	-27.741	0.147
	Aqueous phase	-624.140	-624.140	-657.147	33.007
Copper (1 1 1) + Linalool	Gas phase	-78.753	-39.386	-40.636	1.249
	Aqueous phase	-618.375	-618.375	-652.095	33.720
Copper (1 1 1) + O-cymene	Gas phase	-43.506	-38.767	-39.882	1.115
	Aqueous phase	-629.133	-629.133	-663.006	33.872
Copper (1 1 1) + terpinene-4-ol	Gas phase	-74.399	-44.825	-46.983	2.158
	Aqueous phase	-620.889	-620.889	-654.682	33.793
Copper (1 1 1) + terpeniol	Gas phase	-91.667	-46.064	-46.990	0.925
	Aqueous phase	-616.070	-616.070	-649.169	33.099
Copper (1 1 1) + terpinolene	Gas phase	-53.174	-44.022	-48.104	4.081
	Aqueous phase	-630.175	-630.175	-663.520	33.345
Copper (1 1 1) + Alpha-terpineol	Gas phase	-86.655	-41.053	-43.976	2.923
	Aqueous phase	-630.830	-630.830	-663.661	32.830

The generally stronger adsorption in the aqueous phase suggests that solvation effects enhance the binding of these molecules to the copper surface. Additionally, the higher deformation energies observed in the aqueous environment indicate considerable structural changes during adsorption, which could impact the adsorption mechanism. Regarding the deformation energy, molecules like gamma-cadinene (3.985 kJ/mol) and terpinolene

(4.081 kJ/mol) exhibit higher deformation energies, suggesting that their adsorption involves more substantial structural modifications. Conversely, molecules such as alpha-pinene (0.160 kJ/mol) and camphene (0.251 kJ/mol) show much lower deformation energies, indicating minimal structural alterations upon adsorption.

Table 7. Calculation of Molecules Properties and Bioactivity Score using Molinspiration Analysis

Molecule	Calculation of Molecule Property									Calculation of Bioactivity score					
	<u>miLogP</u>	<u>TPSA</u>	natom s	MW	nON	nOHN H	nviolation s	nroth	<u>volume</u>	GPCR ligand	Ion channel modulator	Kinase inhibitor	Nuclear receptor ligand	Protease inhibitor	Enzyme inhibitor
Alpha-pinene	3.54	0.00	10	136.24	0	0	0	0	151.81	-0.48	-0.43	-1.50	-0.62	-0.85	-0.34
Alpha-terpinolene	3.67	0.00	10	136.24	0	0	0	0	156.72	-0.88	-0.41	-1.61	-0.50	-1.74	-0.26
Alpha-thujene	3.31	0.00	10	135.24	0	0	0	1	151.81	-0.86	-0.37	-1.73	-0.86	-0.82	-0.48
Beta-caryophyllene	4.14	12.53	16	220.36	1	0	0	0	234.01	-0.08	0.14	-0.86	0.62	0.00	0.57
Beta-myrcene	3.99	0.00	10	136.24	0	0	0	4	162.24	-1.11	-0.33	-1.51	-0.45	-1.31	-0.07
Borneol acetate	3.05	26.30	14	196.29	2	0	0	2	202.23	-0.32	-0.33	-1.33	-0.59	-0.44	-0.12
Camphene	3.33	0.00	10	136.24	0	0	0	0	152.37	-1.02	-0.55	-1.85	-1.15	-1.40	-0.82
Eucalyptol (Cineol)	2.72	9.23	11	154.25	1	0	0	0	166.66	-0.93	0.01	-1.60	-1.07	-0.90	-0.15
Gamma-terpinene	3.36	0.00	10	136.24	0	0	0	1	156.74	-0.90	-0.24	-1.37	-0.33	-1.55	-0.07
Gamma-cadinene	5.75	0.00	15	204.36	0	0	1	1	230.30	-0.21	0.11	-0.80	0.27	-0.73	0.27
Humulene	5.75	0.00	15	204.36	0	0	1	1	230.30	-0.21	0.11	-0.80	0.27	-0.73	0.27
Isoborneol	2.35	20.23	11	154.25	1	1	0	0	165.72	-0.47	-0.51	-1.57	-0.84	-0.80	-0.23
Linalool	3.21	20.23	11	154.25	1	1	0	4	175.59	-0.73	0.07	-1.26	-0.06	-0.94	0.07
O-cymene	3.38	0.00	10	134.22	0	0	0	1	150.55	-1.09	-0.54	-1.35	-1.14	-1.37	-0.71
Terpinen-4-ol	2.60	20.23	11	154.25	1	1	0	1	170.65	-0.56	-0.04	-1.68	-0.20	-0.92	0.06
Terpinolene	3.67	0.00	10	136.24	0	0	0	0	156.72	-0.88	-0.41	-1.61	-0.50	-1.74	-0.26
Beta-thujene	3.24	0.00	10	136.24	0	0	0	1	151.84	-0.96	-0.52	-1.79	-1.13	-1.02	-0.58
Terpineol	2.60	20.23	11	154.25	1	1	0	1	170.65	-0.51	0.15	-1.45	-0.02	-0.78	0.14
Alpha-terpineol	2.60	20.23	11	154.25	1	1	0	1	170.65	-0.51	0.15	-1.45	-0.02	-0.78	0.14

Table 8. Results of Osiris calculations of all of the molecules that constitute the REO

Molecule	Calculation of Toxicity Risks, Druglikenes And Drug-Score	Molecule	Calculation of Toxicity Risks, Druglikenes and Drug-Score	Molecule	Calculation of Toxicity Risks, Druglikenes and Drug-Score
Alpha-pinene		Alpha-thujene		Beta-thujene	
Linalol		Beta-myrcene		Camphene	
Eucalyptol (cinéol)		Terpinolén		O-cymene	
Gamma-terpinene		alpha-terpinolène		isoborneol	
terpinen-4-ol		terpineol		Borneol acetate	
beta-caryophyllen		Humulene		Gamma-cadinene	
Alpha-terpineol					

**WAFAA ZRIOUEL, HASSAN MABRAK, MOHAMMED OUBAHOU, AZIZ BENTIS,
BELKHEIR HAMMOUTI**

In general, the results for the other molecules of REO reveal that those with close adsorption energy values suggest a comparable potential for corrosion inhibition. Molecules such as beta-myrcene and beta-caryophyllene, with moderate adsorption energies of -46.321 kJ/mol and -49.086 kJ/mol, respectively, indicate that they can provide some level of protection against corrosion. Similarly, terpinene and terpinolene, despite having lower adsorption energies than gamma-cadinene, still demonstrate significant interaction with the copper surface, with values of -74.399 kJ/mol and -53.174 kJ/mol, respectively. This clustering of adsorption energy values among these molecules implies that they may exhibit similar adsorption characteristics, potentially leading to synergistic effects when used together in corrosion protection formulations. Overall, the close energy values, of molecules, suggest they could contribute to a comprehensive corrosion inhibition mechanism when combined with stronger agents like gamma-cadinene, humulene, and alpha-terpineol.

3.5 POM analysis results

The Molinspiration analysis provides valuable insights into the molecular properties and bioactivity of REO components. Parameters such as miLogP (lipophilicity), TPSA (Topological Polar Surface Area), molecular weight (MW), the number of hydrogen bond acceptors (nON) and donors (nOHNH), violations of Lipinski's rule of five, and the number of rotatable bonds (nrotb) are calculated to evaluate each molecule's potential reactivity and adsorption on metal surfaces. These properties are important for understanding how the molecules interact with surfaces to form protective layers that inhibit corrosion. Table 7 presents the Molinspiration results for all studied molecules.

The OSIRIS results, mentioned in Table 8, reveal that the majority of the molecules exhibit low toxicity risks, with no significant concerns for mutagenicity, tumorigenicity, or reproductive toxicity. Out of the 19 molecules, 13 are considered non-harmful, reinforcing the suitability of REO as an environmentally safe inhibitor. Some molecules show minor irritancy risks, but these are not severe, indicating a favorable safety profile. The Topological Polar Surface Area (TPSA) results play a principal role in understanding the interactions of the REO molecules with metal

surfaces in aqueous environments. Molecules with higher TPSA values, such as borneol acetate (26.30 Å²), isoborneol (20.23 Å²), terpineol (20.23 Å²), alpha-terpineol (20.23 Å²), linalool (20.23 Å²), and terpinen-4-ol (20.23 Å²), show greater potential for forming hydrogen bonds, enhancing their interaction with the metal surface and likely making them more effective corrosion inhibitors [87-88]. The increased reactivity associated with higher TPSA facilitates adsorption and the formation of a protective layer on the metal, effectively inhibiting corrosion. Functional groups like hydroxyls contribute to this inhibition by promoting stronger bonding with the metal surface. In contrast, molecules such as alpha-pinene, beta-myrcene, gamma-terpinene, and camphene, which have a TPSA of 0, show limited hydrogen-bonding capacity and possibly lower inhibition potential, though they may still contribute through hydrophobic interactions [89-90].

4. Conclusions

The corrosion inhibition of REO is due to the combined effect of its various components, with each computational method highlighting different key contributors. Eucalyptol, the main component, plays an important role in forming a protective layer on metal surfaces. Quantum chemical analysis identified alpha-thujene, beta-myrcene, and alpha-pinene as important due to their favorable electronic properties, while Mulliken analysis pointed to oxygenated compounds like alpha-terpineol for their strong inhibition potential. Monte Carlo simulations highlighted gamma-cadinene as the most effective inhibitor, showing high adsorption energy and strong interaction with copper surfaces. These results suggest that REO's inhibitory effect comes from the combined action of multiple molecules rather than a single compound. This synergy makes REO a promising green corrosion inhibitor. Further experimental and electrochemical studies are needed to confirm these computational findings and evaluate REO's performance in different environments.

Acknowledgment

The author declares that no specific support or contributions were received in the preparation of this article.

References

- [1] C. Sakib-uz-zaman, M.A.H Khondoker, A review on extrusion additive manufacturing

WAFAA ZRIOUEL, HASSAN MABRAK, MOHAMMED OUBAHOU, AZIZ BENTIS,
BELKHEIR HAMMOUTI

- of pure copper, Metals. (Basel) 13 (5) (2023) 859.
- [2] S.El Harrari, S.Ayoub, D.Takky, Y.Naimi, Electrochemical Investigation of Terbinafine ($C_{21}H_{25}N$) as a Corrosion Inhibitor for Copper in a Molar Sulfuric Acid Solution. Egypt. J. Chem. 66 (6) (2023) 487 – 492.
- [3] Z.E. Xiao, J. Chen, J. Liu, T.X. Liang, Y. Xu, C.J. Zhu, S.W. Zhong, Microcrystalline copper foil as a high-performance collector for lithium-ion batteries, J. Power Sources 438 (2019) 226973.
- [4] I.Hamidah, A.Solehudin, A.Hamdani, L.Hasanah, K.Khairurrijal, T. Kurniawan, R.Mamat, R.Maryanti, A.B.Dani Nandiyanto, B.Hammouti, Corrosion of copper alloys in KOH, NaOH, NaCl, and HCl electrolyte solutions and its impact to the mechanical properties, Alexandria Engineering Journal 60 (2) (2021) 2235-2243.
- [5] S.El Harrari, A.Salim, D.Takky, Y. Naimi, Corrosion inhibition effect of expired ibuprofen drug on copper in sulfuric acid solution. J. Electrochem. Sci. Eng. 13 (6) (2023) 1005-1013.
- [6] A. Dafali, B. Hammouti, R. Touzani, S. Kertit, A. Ramdani, K. El Kacemi, Corrosion inhibition of copper in 3 per cent NaCl solution by new bipyrazolic derivatives, Anti-Corrosion Methods and Materials 49 (2) (2002) 96-104.
- [7] J. Peng, B. Chen, Z. Wang, J. Guo, B. Wu, S. Hao, Q. Zhang, L. Gu, Q. Zhou, Z. Liu, S. Hong, S. You, A. Fu, Z. Shi, H. Xie, D. Cao, C. Lin, G. Fu, L. Zheng, Y. Jiang, N. Zheng, Surface coordination layer passivates oxidation of copper, Nature 586 (2020) 390–394,
- [8] Q.Li, X.Liu, W.Wang, Corrosion resistance and forming mechanism of phytic acid conversion film on copper foil prepared by electrolysis. Colloids and Surfaces A: Physicochemical and Engineering Aspects 704 (2025) 135504.
- [9] J.Zeng, T.Ling, X.Li, B.Tan, R.Chen, J.Wei, W.Li, Enhanced corrosion inhibition performance of 5-amino-3-bromo-1-methylindazole on copper in sulfuric acid environments. Journal of Molecular Structure 1321 (2025) 140039.
- [10] K. Barouni, A. Kassale, A. Albourine, O. Jbara, B. Hammouti, L. Bazzi, Amino acids as corrosion inhibitors for copper in nitric acid medium: Experimental and theoretical study, J. Mater. Environ. Sci 5 (2) (2014) 456-463.
- [11] A. Bouayad, M. Zerrouk, R. Salim, M. Errajy, A. Ali Raza, K. Azzaoui, B. Hammouti, R. Ouarsal, M. Lachkar, $Ba(H_2PO_3)_2 \cdot 0.5H_2O$: Synthesis, crystal structure optimization, vibrational study, DFT computation and application as a corrosion inhibitor. Mor. J. Chem., 12 (4) (2024) 1575-1595.
- [12] N. Chaubey, A. Qurashi, D.S. Chauhan, M.A. Quraishi, Frontiers and advances in green and sustainable inhibitors for corrosion applications: a critical review, J. Mol. Liq. 321 (2021) 114385.
- [13] W. Daoudi, A. El Aatiaoui, N. Falil, M. Azzouzi, A. Berisha, L.O. Olasunkanmi, O. Dagdag, E.E. Ebenso, M. Koudad, A. Aouinti, M. Loutou, A. Oussaid, Essential oil of *Dysphania ambrosioides* as a green corrosion inhibitor for mild steel in HCl solution, J. Mol. Liq. 363 (2022) 119839.
- [14] R. Ihamdane, M. Tiskar, B. Outemsaa, L. Zemat, O. Dagdag, A. Berisha, E. Berdimurodov, E.E. Ebenso, A. Chaouch, Essential oil of *origanum vulgare* as a green corrosion inhibitor for carbon steel in acidic medium, Arab J Sci Eng. 48 (2023) 7685–7701.
- [15] R.T. Loto, Corrosion inhibition effect of non-toxic α -amino acid compound on high carbon steel in low molar concentration of hydrochloric acid, J. Mater. Res. Techn. 8 (1) (2019) 484-493.
- [16] A. Zarrouk, B. Hammouti, S.S. Al-Deyab, R. Salghi, H. Zarrok, C. Jama, F. Bentiss, Corrosion inhibition performance of 3, 5-diamino-1, 2, 4-triazole for protection of copper in nitric acid solution, International Journal of Electrochemical Science 7 (7) (2012) 5997-6011.
- [17] J. Dai, X. An, Corrosion inhibition properties of *Camellia chrysantha* flower extract for Q235 in 1 M HCl solution, Int. J. Electrochem. Sci. 18 (4) (2023) 100080.
- [18] B. Liao, S. Ma, S. Zhang, X. Li, R. Quan, S. Wan, X. Guo, *Fructus cannabis* protein extract powder as a green and high effective

WAFAA ZRIOUEL, HASSAN MABRAK, MOHAMMED OUBAHOU, AZIZ BENTIS,
BELKHEIR HAMMOUTI

- corrosion inhibitor for Q235 carbon steel in 1 M HCl solution, Int. J. Biol. Macromol. 239 (2023) 124358.
- [19] X. Zhang, L. Yang, Y. Zhang, B. Tan, X. Zheng, W. Li, combined electrochemical/surface and theoretical assessments of *Rosa laevigata* extract as an eco-friendly corrosion inhibitor for copper in acidic medium, J. Taiwan Inst. Chem. Eng. 136 (2022) 104408.
- [20] A. Rizi, A. Sedik, A. Acidi, K. Otmene Rachedi, H. Ferkous, M. Berredjem, A. Delimi, A. Abdennouri, M. Alam, B. Ernst, Y. Benguerba, Sustainable and green corrosion inhibition of mild steel: insights from electrochemical and computational approaches, ACS Omega 8 (49) (2023) 47224–47238.
- [21] W. Zriouel, A. Bentis, S. Majid, B. Hammouti, S. Gmouh, P.S. Umoren, S.A. Umoren, The Blue Tansy Essential Oil–Petra/Osiris/ Molinspiration (POM) Analyses and Prediction of Its Corrosion Inhibition Performance Based on Chemical Composition. Sustainability, 15 (2023) 14274.
- [22] G. Fekkar, F. Yousfi, H. Elmsellem, M. Aiboudi, M. Ramdani, I. Abdel-Rahman, B. Hammouti, L. Bouyazza, Eco-friendly *Chamaerops humilis* L. fruit extract corrosion inhibitor for mild steel in 1 M HCl, International Journal of Corrosion and Scale Inhibition. 9 (2020) 446–459.
- [23] I. El Mounsi, H. Elmsellem, A. Aouniti, H. Bendaha, M. Mimouni, T. Benhadda, R. Mouhoub, B. El Mahi, A. Salhi, B. Hammouti, Hexane extract of *Nigella sativa* L as eco-friendly corrosion inhibitor for steel in 1 M HCl medium, Der Pharm. Chem. 7 (2015) 350–356.
- [24] A. M. Eid, N. Jaradat, L. Issa, A. Abu-Hasan, N. Salah, M. Dalal, A. Mousa, A. Zarour, Evaluation of anticancer, antimicrobial, and antioxidant activities of rosemary (*Rosmarinus Officinalis*) essential oil and its Nanoemulgel. European Journal of Integrative Medicine 55 (2022) 102175.
- [25] M. Rafya, N. Zehhar, A. Hafidi, F. Benkhalti, Review of *Rosmarinus officinalis* L. essential oil, hydrosol, and residues analysis: Composition, bioactivities, and valorization. Industrial Crops & Products 221 (2024) 119392.
- [26] E. Becera, E.M. Altundag, M. Guran, H. S. Vatansever, S. Usturk, D. Y. Hanoglu, K. H. Can Baser, Composition and antibacterial, anti-inflammatory, antioxidant, and anticancer activities of *Rosmarinus officinalis* L. essential oil. South African Journal of Botany 160 (2023) 437–445.
- [27] K. Diass, F. Brahmi, O. Mokhtari, S. Abdellaoui, B. Hammouti, Biological and pharmaceutical properties of essential oils of *Rosmarinus officinalis* L. and *Lavandula officinalis* L. Materials Today: Proceedings 45 (2021) 7768–7773.
- [28] B. A. Al Jahdaly, *Rosmarinus officinalis* extract as eco-friendly corrosion inhibitor for copper in 1 M nitric acid solution: Experimental and theoretical studies. Arabian Journal of Chemistry 16 (2023) 104411.
- [29] W. Daoudi, O. Dagdag, C. Verma, E. Berdimurodov, A. Oussaid, A. Berisha, A. Oussaid, M. Abboud, A. El Aatiaoui, *Rosmarinus officinalis* L. Oil as an Eco-Friendly corrosion inhibitor for mild steel in acidic Solution: Experimental and computational studies. Inorganic Chemistry Communications 161 (2024) 112030.
- [30] R.T. Loto, C.A. Loto, M. Fajobi, G. Olanrewaju, Comparative assessment and statistical data of admixed rosemary and castor oil on the corrosion inhibition of high carbon and P4 low carbon mold steels. Materials Today: Proceedings 49 (2022) 1926–1931.
- [31] U.R. Juergens, U. Dethlefsenw, G. Steinkamp, A. Gillissen R. Repges, H. Vetter, Anti-inflammatory activity of 1,8-cineol (eucalyptol) in bronchial asthma: a double-blind placebo-controlled trial. Respiratory medicine 97 (2003) 250–256.
- [32] U.R. Juergens, M. Stoßer, H. Vetter, Inhibition of cytokine production and arachidonic acid metabolism by eucalyptol (1,8-cineol) in human blood monocytes in vitro. Eur J Med Res 3 (1998) 508–510.
- [33] U.R. Juergens, M. Stoßer, N. Vetter, Steroid-like inhibition of monocyte arachidonic acid metabolism and IL-1 β production by eucalyptol (1,8-cineol) (in German). Atemw-Lungenkrkh 24 (1998) 3–11.

WAFAA ZRIOUEL, HASSAN MABRAK, MOHAMMED OUBAHOU, AZIZ BENTIS,
BELKHEIR HAMMOUTI

- [34] N. Arrouse, E.H. Mabrouk, B. Hammouti, F. El-Hajjaji, Z. Rais, M. Taleb, New strategy of synthesis, characterization, theoretical study and inhibition effect on mild steel corrosion in acidic solution, *Mediterranean Journal of Chemistry* 10 (5) (2020) 477-491.
- [35] S. Zarougui, M. Er-rajy, A. Faris, H. Imtara, M. El fadili, O. Al kamaly, S.Z. Alshawwa, F.A. Nasr, M. Aloui, M. Elhallaoui, QSAR, DFT studies, docking molecular and simulation dynamic molecular of 2-styrylquinoline derivatives through their anticancer activity. *Journal of Saudi Chemical Society* 27 (2023) 101728.
- [36] Material studio version 2020. B. Delley, *J. Chem. Phys.* 113, 7756 (2000).
- [37] M. Er-rajy, M. El fadili, S. Mujwar, H. Imtara, O. Al kamaly, S. Z. Alshaww, F.A. Nasr, S. Zarougui, M. Elhallaoui. Design of novel anti-cancer agents targeting COX-2 inhibitors based on computational studies. *Arabian Journal of Chemistry* 16 (2023) 105193.
- [38] M. Oubahou, M. Rbaa, D. Takky, Y. Naimi, A.A. Alrashdi, H. Lgaz, Elucidating the role of novel halogenated hydroquinazolinone derivatives in mitigating copper corrosion in saline conditions: A joint assessment of experimental outcomes and computational analysis. *Journal of Molecular Liquids* 390 (2023) 122966.
- [39] M. Oubahou, A. El aloua, N. Benzbiria, S. El Harrari, D. Takky, Y. Naimi, A. Zeroual, Shifa Wang, A. Syed, M.E. Belghiti. Electrochemical, thermodynamic and computational investigation of the use of an expired drug as a sustainable corrosion inhibitor for copper in 0.5 M H₂SO₄. *Materials Chemistry and Physics*, 323 (2024) 129642.
- [40] W. Zriouel, A. Bentis, S. Majid, B. Hammouti, S. Gmouh, Blue Tansy essential oil as eco-friendly corrosion inhibitor of mild steel in 1 M HCl solution: Electrochemical study, DFTB computation and Monte Carlo simulation. *Int. J. Corros. Scale Inhib.* 12 (3) (2023) 1139-1161.
- [41] M. Er-rajy, M. El Fadili, H. Hadni, N. Naceiri Mrabti, S. Zarougui, M. Elhallaoui, 2D-QSAR modeling, drug-likeness studies, ADMET prediction, and molecular docking for anti-lung cancer activity of 3-substituted-5-(phenylamino) indolone derivatives. *Struct Chem* 33 (2022) 973-986.
- [42] R. Meena, A.R. Khandelwal, K. Sharma, N. Khatik, H. Singh, S. Khaturia, H. Sachdev, rGO/CuO NC catalyzed green synthesis, DFT studies, Mulliken atomic charge analysis and anti-inflammatory activity of indole derivatives. *Journal of Organometallic Chemistry* 1019 (2024) 123322.
- [43] A. Kasprzhitskii, G. Lazorenko, Corrosion inhibition potential of sulfur-containing and aromatic amino acids on magnesium in Hank's solution. *Colloids and Surfaces A: Physicochemical and Engineering Aspects* 703 (2024) 135267.
- [44] A. Guendouz, N. Missoum, A. Chetouani, S. S. Al-Deyab, B. Ben Cheikhe, N. Boussala, B. Hammouti, M. Taleb, A. Aouniti, Quantum Chemical Studies on the Inhibiting Effect of New Synthesized Bipyrazols of C38 Steel Corrosion in 1M HCl. *Int. J. Electrochem. Sci.*, 8 (2013) 4305 - 4327.
- [45] X. Meng, Q. Zhang, X. Lv, J. Chen, Y. Peng, P. Dong, Q. Sun, Corrosion inhibition effect of several amino acids on an Al-Zn-Mg-Cu alloy: Electrochemical study, DFT and MD simulation, *Materials Today Communications*, 41 (2024) 110529.
- [46] C. Verma, H. Lgaz, D.K. Verma, Eno E. Ebenso, I. Bahadur, M.A. Quraishi, Molecular dynamics and Monte Carlo simulations as powerful tools for study of interfacial adsorption behavior of corrosion inhibitors in aqueous phase: A review. *Journal of Molecular Liquids* 260 (2018) 99-120.
- [47] W. Zriouel, A. Bentis, S. Majid, B. Hammouti, S. Gmouh, Computational study and predictive investigation of the inhibitory behavior of Geranium essential oil: DFT calculation, Monte Carlo simulation and POM analyses. *Eur. Chem. Bull.* 12 (12) (2023) 2978-3002
- [48] S. Sun, Y. Geng, L. Tian, S. Chen, Y. Yan, S. Hu, Density functional theory study of imidazole, benzimidazole and 2-mercaptobenzimidazole adsorption onto clean Cu (111) surface. *Corros. Sci.* 63 (2012) 140-147.
- [49] M. Oubahou, M. Rbaa, H. Lgaz, D. Takky, Y. Naimi, A. A. Alrashdi, H. Lee, Exploring

**WAFAA ZRIOUEL, HASSAN MABRAK, MOHAMMED OUBAHOU, AZIZ BENTIS,
BELKHEIR HAMMOUTI**

- sustainable corrosion inhibition of copper in saline environment: An examination of hydroquinazolinones via experimental and ab initio DFT simulations. *Arabian Journal of Chemistry* 17 (2024) 105716.
- [50] R.H. Hama Salih, A.H. Hasana , N.H. Hussen , F.E. Hawaiz , T.Ben Hadda , J. Jamalis, F.A. Almalkif , A.S. Adeyinka , Louis-Charl C. Coetzee , A.K. Oyebamiji, Thiazole-pyrazoline hybrids as potential antimicrobial agent: Synthesis, biological evaluation, molecular docking, DFT studies and POM analysis. *Journal of Molecular Structure* 1282 (2023) 135191.
- [51] K.O. Rachedi, T. Sothea Ouk, R. Bahadi, A. Bouzina, S.E. Djouad, K. Bechlem, R. Zerrouki, T. Ben Hadda, F. Almalki, M. Berredjem, DFT Study, POM analyses and molecular docking of novel oxazaphosphinanes: identification of antifungal pharmacophore site, *J. Mol. Struct.* 106 (2019) 196–203,
- [52] K. Bechlem, M. Berredjem, S.E. Djouad, T.O. Sothea, S. Bouacida, C. Marminon, T. Ben Hadda, J. Lebreton, A. Bouzina, Novel N-acylsulfamoyl-oxazolidin-2-ones: Synthesis, antitumor activity, X-ray crystallographic study, molecular docking and POM analyses. *Journal of Molecular Structure* 1262 (2022) 132935.
- [53] R. Sabbahi, M. H. Youssoufi , K. Azzaoui, B. Hammouti, A. Chetouani, Sanaa Saiabi, H. Zgou. Computational POM and DFT evaluation of phycocyanin and its derivatives as a potential anticancer agent. *Materials Today: Proceedings* 72 (2023) 3669–3676.
- [54] S. Bawazer, A. Khan, A. Rauf, T. Hadda, Y. Al-Awthan, O. Bahattab, U. Rashid, I. Khan, M. Nawaz, M. Uddin, O. Ahmed, M. Shariati, POM analysis and computational interactions of 8-hydroxydiospyrin inside active site of protein tyrosine phosphatase 1B, *BIOCELL* 45 (2021) 751.
- [55] H. Murad, T. Alqurashi, Eucalyptol potentiates antianginal effect while blunts tachycardia of nifedipine in rats via nitric oxide, antioxidant, and anti-inflammatory pathways: In vivo and in vitro study. *Journal of Functional Foods* 113 (10) (2024) 106019.
- [56] K. Hac-Wydro, K. Szydło, The influence of environmentally friendly pesticide – Eucalyptol – alone and in combination with terpinen-4-ol – on model bacterial membranes. *Colloids and Surfaces B: Biointerfaces* 146 (2016) 918-923.
- [57] A. K Dhakad , V. V Pandey , S. Beg , J.M Rawat , A.Singh, Biological, medicinal and toxicological significance of Eucalyptus leaf essential oil: a review. *J. Sci. Food Agric.* 98 (3) (2018) 833–848.
- [58] C.C. Hoch, J. Petry, L. Griesbaum, T. Weiser, K. Werner, M. Ploch, A. Verschoor, G. Multhoff, A.B. Dezfouli, B. Wollenberg, 1,8-cineole (eucalyptol): A versatile phytochemical with therapeutic applications across multiple diseases. *Biomedicine & Pharmacotherapy* 167 (2023) 115467.
- [59] V. Nagarajan, R. Bhuvaneswari, R. Chandiramouli, Adsorption studies of camphene and eucalyptol molecules on orthorhombic germanane nanosheet - A first-principles investigation. *Journal of Molecular Graphics and Modelling* 119 (2023) 108395.
- [60] Z. Zarei , M. Kharaziha , F. Karimzadeh , E. Khadem, Synthesis and biological applications of nanocomposite hydrogels based on the methacrylation of hydroxypropyl methylcellulose and lignin loaded with alpha-pinene. *Carbohydrate Polymers* 346 (2024) 122642.
- [61] T. Mochida, R. Ohnishi, N. Horita, Y. Kamiya, T. Okuhara, Hydration of α -pinene over hydrophobic zeolites in 1,4-dioxane-water and in water. *Microporous and Mesoporous Materials* 101 (2007) 176–183.
- [62] Y. Zhou , J. Wang , X. Wang , F. Wang , X. Li, Efficient production of α -pinene through identifying the rate-limiting enzymes and tailoring inactive terminal of pinene synthase in *Escherichia coli*. *Fuel* 343 (2023) 127872.
- [63] R. Liang, BG. Harvey, RL. Quintana, JM. Suflita, Assessing the Biological Stability of a Terpene-Based Advanced Biofuel and Its Relationship to the Corrosion of Carbon Steel. *Energy Fuel* 29 (2015) 5164–5170.
- [64] S. Cherrad, A.A. Alrashdi, HS. Lee, Y. El aoufir, H. Lgaz, B. Satrani, M. Ghanmi , El M. Aouane , A. Chaouch, Cupressus arizonica fruit essential oil: A novel green inhibitor for acid corrosion of carbon steel.

WAFAA ZRIOUEL, HASSAN MABRAK, MOHAMMED OUBAHOU, AZIZ BENTIS,
BELKHEIR HAMMOUTI

- Arabian Journal of Chemistry 15 (2022) 103849.
- [65] AE. Al-Shudifat, E. Qnais, Y. Bseiso, M. Wedyan, O. Gammoh, M. Alqudah, Ad. M. Bani Khaled, A. Alqudah, Antidepressant potential of β -caryophyllene in maternal separation-induced depression-like in mice: A focus on oxidative stress and nitrite levels. *Phytomedicine Plus* 4 (2024) 100624.
- [66] S. Pei, J. Chen, J. Lu, L. Yao, N. Zhang, Exploring the physiological response differences of β -caryophyllene, linalool and citral inhalation and their anxiolytic potential, *Heliyon* 10 (2024) e38941.
- [67] F. Akman, A. Demirpolat, A.S. Kazachenko, N. Issaoui, O. Al-Dossary, Molecular Structure, Electronic Properties, Reactivity (ELF, LOL, and Fukui), and NCI-RDG Studies of the Binary Mixture of Water and Essential Oil of *Phlomis bruguieri*. *Molecules* 28 (2023) 2684.
- [68] Y. Yang, Y. Wang, M.-X. Li, T. Wang, D. Wang, C. Wang, M. Zha, H.-Y. Wang, Recent progress in self-repairing coatings for corrosion protection on magnesium alloys and perspective of porous solids as novel carrier and barrier, *J. Magnes. Alloy*. 11 (2023) 3585–3608.
- [69] Z. El Adnani, M. MchaRfilmi, M. Sfaira, M. Benzakour, A.T. Benjelloun, M. Ebn Touhami, DFT theoretical study of 7-R-3methylquinoxalin-2(1H)-thiones (RH; CH₃; Cl) as corrosion inhibitors in hydrochloric acid, *Corros. Sci.* 68 (2013) 223–230.
- [70] N.A. Chikaodili, C.S. Ume, P.C. Nnaji, N. B. Iroha, O. Dagdag, J.O. Ezeugo, A. Thakur, V.C. Anadebe, O.D. Onukwuli, Physisorption or chemisorption: Insight from AI computing model based on DFT, MC/MD-simulation for prediction of MOF-based inhibitor adsorption on Cu in brine solution. *Computational and Theoretical Chemistry* 1238 (2024) 114730.
- [71] M. S. ahin, G. Gece, F. Karci, S. Bilgiç, Experimental and theoretical study of the effect of some heterocyclic compounds on the corrosion of low carbon steel in 3.5% NaCl medium, *J. Appl. Electrochem.* 38 (2008) 809–815,
- [72] A.K. Singh, B. Chugh, S. Kr Saha, P. Banerjee, E.E. Ebenso, S. Thakur, B. Panie, Evaluation of anti-corrosion performance of an expired semi synthetic antibiotic cefdinir for mild steel in 1 M HCl medium: an experimental and theoretical study, *Results Phys.* 14 (2019) 102383.
- [73] M. Bouassiria, M. El Faydy, F. Benhiba, T. Laabaissi, H. Fakhry, S. Saoiabi, R. Tour, I. Warad, A. Guenbour, B. Lakhri, H. Oudda, A. Zarrouk, Corrosion effectiveness of 5-(4-Phenylpiperazin-1-yl) methyl quinolin-8-ol for carbon steel in 1.0 M HCl, *J. Bio- Tribo-Corros.* 8 (2) (2022) 1–15.
- [74] R.G. Pearson, Absolute electronegativity and hardness: application to inorganic chemistry, *Inorg. Chem.* 27 (1988) 734–740,
- [75] W. Wang, D. Chen, F. Li, X. Xiao, Q. Xu, Metal-organic framework-based materials as platforms for energy applications, *Chem* 10 (1) (2024) 86-133.
- [76] X. Meng, Q. Zhang, X. Lv, J. Chen, Y. Peng, P. Dong, Q. Sun, Corrosion inhibition effect of several amino acids on an Al-Zn-Mg-Cu alloy: Electrochemical study, DFT and MD simulation. *Materials Today Communications* 41 (2024) 110529.
- [77] H. Hamani, D. Daoud, S. Benabid, T. Douadi. Electrochemical, density functional theory (DFT) and molecular dynamic (MD) simulations studies of synthesized three new Schiff bases as corrosion inhibitors on mild steel in the acidic environment. *Journal of the Indian Chemical Society* 99 (2022) 100492.
- [78] L. Boucherit, T. Douadi, N. Chafai, M. Al-Noaimi, S. Chafaa, The inhibition activity of 1, 10-bis (2-formylphenyl)-1, 4, 7, 10-tetraoxadecane (Ald) and its Schiff base (L) on the corrosion of carbon steel in HCl: experimental and theoretical studies, *Int. J. Electrochem. Sci.* 13 (2018) 3997–4025.
- [79] H. Debab, T. Douadi, D. Daoud, S. Issaadi, S. Chafaa, Electrochemical and quantum chemical studies of adsorption and corrosion inhibition of two new Schiff bases on carbon steel in hydrochloric acid media, *Int. J. Electrochem. Sci.* 13 (2018) 6958–6977.
- [80] S.G. Gounhalli, S. Basavaraj, S.M. Hanagodimath, Spectroscopic analysis of NMR, IR, Raman and UV-Visible, HOMO-LUMO, ESP and Mulliken charges of coumarin derivative by density functional

**WAFAA ZRIOUEL, HASSAN MABRAK, MOHAMMED OUBAHOU, AZIZ BENTIS,
BELKHEIR HAMMOUTI**

- theory, J. Maharaja Sayajirao Univ. Baroda 55 (1 (XIV)) (2021) 213–229.
- [81] I.B. Obot, D.D. Macdonald, Z.M. Gasem, Density functional theory (DFT) as a powerful tool for designing new organic corrosion inhibitors: Part 1: An overview, *Corros. Sci.* 99 (2015) 1–30,
- [82] L.O. Olasunkanmi, I.B. Obot, E.E. Ebenso, Adsorption and corrosion inhibition properties of N-{n-[1-R-5-(quinoxalin-6-yl)-4,5- dihydropyrazol- 3 yl] phenyl} methane sulfon amides on mild steel in 1 M HCl: experimental and theoretical studies, *RSC Adv.* 6 (2016) 86782–86797.
- [83] A. Kasprzhitskii, G. Lazorenko. Corrosion inhibition potential of sulfur-containing and aromatic amino acids on magnesium in Hank's solution. *Colloids and Surfaces A: Physicochemical and Engineering Aspects* 703 (2024) 135267.
- [84] H. Lgaz, R. Salghi, M. Larouj, M. Elfaydy, S. Jodeh, H. Abbout, B. Lakhri, K. Toumiat, H. Oudda, Corrosion inhibition of mild steel in hydrochloric acid by 5,5',5''-(nitrilotris (methylene)) tris-(8-quinolinol) : Experimental, theoretical and molecular dynamic studies. *Mor. J. Chem.* 4 N°2 (2016) 592-612.
- [85] S. John, R. Jeevana, K.K. Aravindakshan, Abraham Joseph, Corrosion inhibition of mild steel by N(4)- substituted thiosemicarbazone in hydrochloric acid media. *Egyptian Journal of Petroleum* 26 (2017) 405-412.
- [86] N. M. EL Basiony, Amr. Elgendya, H. Nadyb, M. A. Migaheda , E. G. Zaki, Adsorption characteristics and inhibition effect of two Schiff base compounds on corrosion of mild steel in 0.5 M HCl solution: experimental, DFT studies, and Monte Carlo simulation. *RSC Adv.*, 9 (2019) 10473-10485.
- [87] M. Dąbrowska, M. Starek, G. Chłon-Rzepa, A. Zagorska, Ł. Komsta, A. Jankowska, M. Slusarczyk, M. Pawłowski, Estimation of the lipophilicity of purine-2,6-dione-based TRPA1 antagonists and PDE4/7 inhibitors with analgesic activity. *Bioorganic & Medicinal Chemistry Letters* 49 (2021) 128318.
- [88] Prasanna S, Doerksen RJ. Topological polar surface area: a useful descriptor in 2D-QSAR. *Curr Med Chem.* 16 (1) (2009) 21-41.
- [89] N. Saghdani, A. El Abbouchi, N. El Brahmi, A. Idir, K. Otmane Rachedi, M. Berredjem , R. Haloui , S. Elkhatabi, H. Ait Mouse , T. Ben Hadda , M. Bousmina, A. Zyad , S. El Kazzouli, Design, synthesis, in-vitro, in-silico, DFT and POM studies of a novel family of sulfonamides as potent anti-triple-negative breast cancer agents. *Computational Biology and Chemistry* 113 (2024) 108214.
- [90] M. Sirajuddin, S. Ali, M Nawaz Tahir, Pharmacological investigation of mono-, di- and tri-organotin (IV) derivatives of carbodithioates: Design, spectroscopic characterization, interaction with SS-DNA and POM analyses. *Inorganica Chimica Acta* 439 (2016) 145-158.